Bone 43 (2008) 55–63

Contents lists available at ScienceDirect

Bone

journal homepage: www.elsevier.com/locate/bone

The study of abnormal bone development in the Apert syndrome Fgfr2$^{+/S252W}$ mouse using a 3D hydrogel culture model

Fan Yang [a], Yingli Wang [b], Zijun Zhang [c], Bryan Hsu [c], Ethylin Wang Jabs [b], Jennifer H. Elisseeff [c,*]

[a] Department of Chemical Engineering, Massachusetts Institute of Technology, 45 Carleton Street, E25-342, Cambridge, MA, 02142, USA
[b] Department of Genetics and Genomic Sciences, Mount Sinai School of Medicine, 1425 Madison Avenue, New York, NY, USA
[c] Department of Biomedical Engineering, The Johns Hopkins University, 3400 N. Charles Street, Clark 106, Baltimore, MD, 21218, USA

ARTICLE INFO

Article history:
Received 30 May 2007
Revised 19 January 2008
Accepted 7 February 2008
Available online 29 February 2008

Keywords:
Tissue engineering
Apert syndrome
FGFR2
Osteoblast
Hydrogel

ABSTRACT

Apert syndrome is caused by mutations in fibroblast growth factor receptor 2 (Fgfr2) and is characterized by craniosynostosis and other skeletal abnormalities. The Apert syndrome Fgfr2$^{+/S252W}$ mouse model exhibits perinatal lethality. A 3D hydrogel culture model, derived from tissue engineering strategies, was used to extend the study of the effect of the Fgfr2$^{+/S252W}$ mutation in differentiating osteoblasts postnatally. We isolated cells from the long bones of Apert Fgfr2$^{+/S252W}$ mice (n=6) and cells from the wild-type sibling mice (n=6) to be used as controls. During monolayer expansion, Fgfr2$^{+/S252W}$ cells demonstrated increased proliferation and ALP activity, as well as altered responses of these cellular functions in the presence of FGF ligands with different binding specificity (FGF2 or FGF10). To better mimic the *in vivo* disease development scenario, cells were also encapsulated in 3D hydrogels and their phenotype in 3D *in vitro* culture was compared to that of *in vivo* tissue specimens. After 4 weeks in 3D culture in osteogenic medium, Fgfr2$^{+/S252W}$ cells expressed 2.8-fold more collagen type I and 3.3-fold more osteocalcin than did wild-type controls (p<0.01). Meanwhile, Fgfr2$^{+/S252W}$ cells showed decreased bone matrix remodeling and expressed 87% less Metalloprotease-13 and 71% less Noggin (p<0.01). The S252W mutation also led to significantly higher production of collagen type I and II in 3D as shown by immunofluorescence staining. *In situ* hybridization and alizarin red S staining of postnatal day 0 (P0) mouse limb sections demonstrated significantly higher levels of osteopontin expression and mineralization in Fgfr2$^{+/S252W}$ mice. Complementary to *in vivo* findings, this 3D hydrogel culture system provides an effective *in vitro* venue to study the pathogenesis of Apert syndrome caused by the analogous mutation in humans.

Introduction

Fibroblast growth factors (FGF) and fibroblast growth factor receptors (FGFR) play critical roles in the process of osteogenesis that occurs in the developing calvarial and long bones [1,2]. In humans, mutations in FGFR1, FGFR2, and FGFR3 were shown to induce craniosynostosis, a congenital disease that is characterized by premature fusion of cranial sutures. One of the most severe forms of craniosynostosis is Apert syndrome, an autosomal dominant disorder characterized by craniofacial anomalies and severe symmetrical syndactyly (fused fingers and toes). The prevalence of this condition is estimated at less than 1 in 65,000 live births and accounts for 4.5% of all cases of craniosynostosis [3,4].

Genetic analysis has revealed that more than 99% of cases with Apert Syndrome arise by specific missense mutations resulting in amino acid substitutions in adjacent residues, Ser252Trp (S252W) and Pro253Arg (P253R), in the linker between the second and third extracellular immunoglobulin domains of FGFR2 [5,6]. These mutations are proposed to cause misregulated tyrosine kinase receptor activity by producing increased ligand affinity and changes in specificity for fibroblast growth factors [7–9]. The S252W mutation affects the two splice forms of FGFR2, b and c, allowing mesenchymal splice form FGFR2c to bind and be activated by the mesenchymal-expressed ligands FGF7 or FGF10, to which FGFR2c does not normally bind [8]. The results of loss of FGFR2 function have suggested a critical role for FGF signaling in pregastrulation mammalian development [10]. Despite these advances in our understanding of FGFR2 mutations, the detailed molecular mechanisms underlying pathogenesis of Apert syndrome remain elusive.

Two groups have created FGFR2 knock-in mutant mice that exhibit features similar to those of human Apert syndrome [11,12]. In our Fgfr2$^{+/S252W}$ mice, a midline sutural defect and craniosynostosis with abnormal osteoblastic proliferation and differentiation was observed in mouse embryos at embryonic day 16.5 to postnatal day 1 [11]. However, due to the early postnatal lethality of this mutation, it is very difficult to analyze the abnormal bone growth in these mice. Therefore, it remains to be understood how the mutations affect tissue development at a more

* Corresponding author. 3400 North Charles Street, Clark Hall, Room 106, Baltimore, MD, 21218, USA. Fax: +1 410 516 8152.
E-mail addresses: fyang4@mit.edu (F. Yang), yingli.wang@mssm.edu (Y. Wang), zhangzj@jhu.edu (Z. Zhang), humbert@jhu.edu (B. Hsu), Ethylin.Jabs@mssm.edu (E.W. Jabs), jhe@jhu.edu (J.H. Elisseeff).

8756-3282/$ – see front matter © 2008 Elsevier Inc. All rights reserved.
doi:10.1016/j.bone.2008.02.008

mature stage. Isolation and culture of cells from these mutant mice under controlled *in vitro* conditions would enable us to perform extended studies of the abnormal tissue development in a more quantitative manner.

Previous *in vitro* studies of Apert mutant cells were performed only in 2D culture, which may not be a realistic representation of how the cells behave in the 3D environment *in vivo* [13,14]. The technology for growing cells in 3D is one of the key techniques in tissue engineering applications. While having been widely used in tissue engineering as a vehicle for tissue repair, this 3D cell culture system has not been well explored as an approach for understanding mechanisms of cell response in disease progression. A rapidly growing body of literature has underscored the importance of physical three-dimensionality of the matrix in regulating cell behavior, including cell proliferation and differentiation [15–21]. Cell–matrix interactions in 3D matrices differ greatly from those characterized on 2D substrates [15,22]. In addition, numerous cancer cell behaviors in 3D culture have been identified that were not present in 2D culture [22].

We previously demonstrated that photopolymerizing poly(ethylene glycol)-diacrylate (PEGDA) hydrogels can be used to encapsulate cells and support bone and cartilage tissue regeneration in a 3D environment [23–25]. In the present study, we isolated cells from the long bones of Apert Fgfr2$^{+/S252W}$ mice, expanded and characterized them in 2D culture, and then examined bone development in 3D using a hydrogel culture model. We report here that the FGFR2$^{+/S252W}$ mutation is associated with increased osteoblastic differentiation, decreased matrix remodeling and abnormal chondrogenesis; and such alterations in cell differentiation may be due in part to changes in the Fgfr2 response to FGF ligands. The consistency of these *in vitro* data and *in vivo* animal model suggests this 3D culture system is an effective *in vitro* tool to study the pathogenesis of Apert syndrome.

Materials and methods

The Fgfr2$^{+/S252W}$ mice

The Apert Fgfr2$^{+/S252W}$ mice were generated as previously reported [11]. Genotyping of tail DNA to distinguish mutant from wild-type progeny was carried out by PCR analysis. Apert Fgfr2$^{+/S252W}$ mice are neonatal lethal and demonstrate significant anomalies including craniosynostosis and multiple bony anomalies, as evidenced by histopathological studies [11]. Skeletal staining with Alizarin Red S and Alcian Blue was performed [26]. Care and use of mice for this study were in compliance with relevant animal welfare guidelines approved by the Johns Hopkins University Animal Care and Use Committee.

Isolation and expansion of cells from the long bones of Fgfr2$^{+/S252W}$ mice

Cells were obtained from the middle shaft of the limbs of Apert newborn (day 0) Fgfr2$^{+/S252W}$ mice (n=6) as previously described (Fig. 1A) [11]. Grossly, the mutant and wild-type mouse limbs exhibit similar morphology, and the mutant mice demonstrated a smaller body size in general [11]. The cells were isolated using 1 mg/ml collagenase D (Boehringer Mannheim) digestion for 2 h, and cultured in DMEM (GIBCO) supplemented with 10% fetal bovine serum, 100 U/ml penicillin and 100 μg/ml streptomycin. By the same procedure, cells were also isolated from wild-type littermates (n=6) and cultured as controls.

Alkaline phosphatase (ALP) and collagen type I staining of monolayer culture: To verify that the cultured cells had characteristics of osteoblasts, passage 1 cells were stained for ALP and collagen type 1. After 4 days in culture, the cells were fixed in 10% formalin for 15 min. For ALP staining, the fixed cells were incubated for 30 min with a staining solution including 0.1 mg/ml naphthol AS-MX (Sigma) and 0.2 mg/ml fast red-violet LB salt (Sigma) in 0.1 M Tris buffer; cells positive for ALP appeared red. For collagen type I staining, immunofluorescence staining was performed using rabbit polyclonal antibodies specific for collagen type I (Research Diagnostics) as the primary antibody and fluorescein (FITC)-conjugated AffiniPure goat anti-rabbit IgG (Jackson ImmunoResearch Lab) as the secondary antibody. In negative control samples, the primary antibody was replaced with PBS.

Cell proliferation, ALP activity kinetics and responses to FGF2 and FGF10 in 2D culture

Cell proliferation

Osteoblasts (passage 1) from Fgfr2$^{+/S252W}$ or wild-type mice were plated in 96-well culture plates at a density of 5000 cells/cm^2. Cells were cultured with 100 μl (per well) of osteoblast medium, with the medium being changed daily. After 4 days of culture, the number of proliferating cells in each well was determined using the CellTiter 96® AQ$_{ueous}$ One Solution cell proliferation assay. This colorimetric assay indirectly quantifies proliferating cells based on bioreduction of a tetrazolium salt by living cells to a colored formazan product. Briefly, CellTiter 96® AQ$_{ueous}$ One Solution 20 μl/well (Promega) was added to the cell-containing wells. The same volume was also added to each of three wells containing medium alone to allow us to calculate the background absorbance from the medium. The samples were incubated for 2 h at 37 °C. Absorbance (490 nm) was read using a μQuant universal microplate spectrophotometer (Bio-Tek Instruments®).

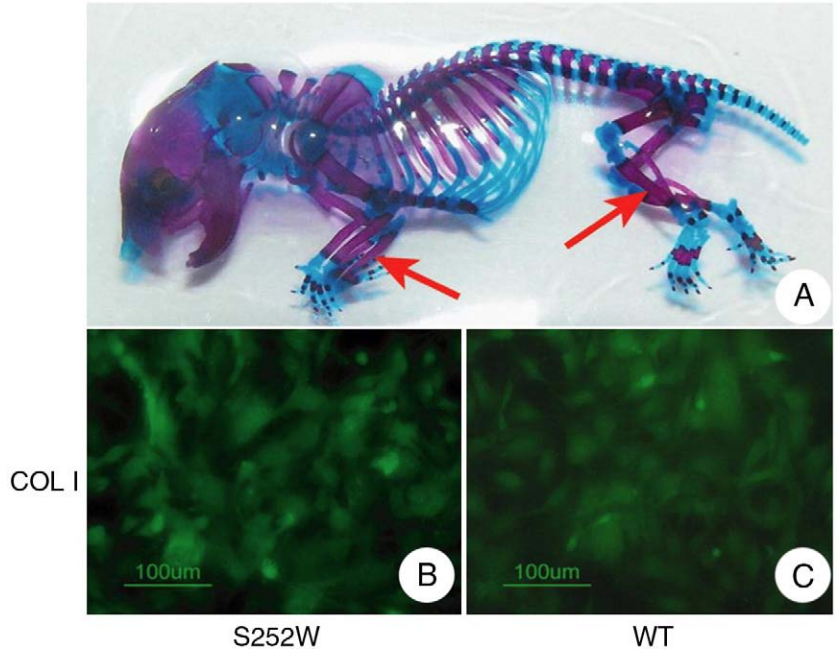

Fig. 1. Stained whole skeleton of the Fgfr2$^{+/S252W}$ mice and the bone marker staining of isolated cells in monolayer. (A, B) mutant; (C) wild-type controls. (A) Mouse skeleton of Fgfr2 $^{+/S252W}$ mice, with bone stained purple (alizarin red S staining) and cartilage stained blue (alcian blue). Osteoblasts were isolated from the middle shaft of the long bones (arrows). (B, C) Immunofluorescence staining of collagen type I demonstrated similar amounts of deposition in both Fgfr2 $^{+/S252W}$ cells and wild-type controls. S252W: Fgfr2$^{+/S252W}$; WT: wild-type. Scale bars: B,C, 100 μm.

Table 1
Mouse primer sequence used in RT-PCR

Gene	Primer sequence	Annealing temperature
Beta actin	F—tggcaccacaccttctacaatgagc	60 °C
	R—gcacagcttctccttaatgtcacgc	
m-Cbfa1	F—gtgcggtgcaaactttctcc	59 °C
	R—aatgactcggttggtctcgg	
m-ON	F—atccagagctgtggcacaca	61 °C
	R—ggaaagaaacgcccgaaga	
m-OPN	F—gatgccacagatgaggacctc	60 °C
	R—ctgggcaacagggatgacat	
m-Col I	F—gcatggccaagaagacatcc	60 °C
	R—cctcgggtttccacgtctc	
m-BSP	F—cagaggaggcaagcgtcact	62 °C
	R—ctgtctgggtgccaacactg	
m-Osteocalcin	F—ccgggagcagtgtgagctta	60 °C
	R—tagatgcgtttgtaggcggtc	
m-Mmp13	F—agttgacaggctccgagaaa	60 °C
	R—ggcactccacatcttggttt	
m-Noggin	F—cggccagcactatctacaca	60 °C
	R—gcgtctcgttcagatccttc	
m-BMP4	F—cgttacctcaagggagtgga	60 °C
	R—atgcttgggactacgtttgg	

ALP activity kinetics

Passage 1 osteoblasts were plated in 6-well culture plates at an initial density of 5000 cells/cm^2. To measure the ALP activity quantitatively, Fgfr2$^{+/S252W}$ or wild-type cells from three wells were harvested by trypsin treatment at a specific time every other day, and the cell number from each well was determined using a Z2 Coulter Particle Count and Size Analyzer. Trypsinized cells were then washed in PBS three times, vortexed in 0.2% Triton X-100 (Sigma) for 5 min, and the supernatants were collected for quantitative ALP assay. ALP reagent was prepared using the Alkaline Phosphatase Substrate Kit (BioRad Laboratories) following the manufacturer's instructions. Absorbance kinetics was recorded at 405 nm using a Beckman DU-530 spectrophotometer and the ALP activity was calculated on the basis of millimolar absorptivity of *p*-nitrophenol. For comparison, the ALP activity was normalized on the basis of cell number.

Responses to FGF2 and FGF10

To examine the effect of FGF2 and FGF10 on cell proliferation and ALP activity, respectively, 10 ng/ml of FGF2 or FGF10 (Research Diagnostics Inc) was added to the culture medium of the Fgfr2$^{+/S252W}$ and wild-type cells over a 10-day culture period. Cell proliferation was evaluated by the CellTiter 96® AQ$_{ueous}$ One Solution cell proliferation assay as described above, and quantitative ALP assays were performed every other day during the 10-day culture period.

Cell encapsulation and tissue development of osteoblasts from Fgfr2$^{+/S252W}$ and wild-type mice in 3D hydrogels

Hydrogel encapsulation

Polymer solution was prepared by dissolving poly(ethylene glycol)-diacrylate (PEGDA; Nektar Therapeutics) in PBS to make a 15% (w/v) hydrogel, with 0.05% (w/v) photoinitiator Igracure D2959 (Ciba Specialty Chemicals) [24]. Osteoblasts (P3) from Fgfr2$^{+/S252W}$ or wild-type mice were homogeneously suspended in the polymer solution to yield a concentration of 1.5×10^7 cells/ml. The cell–polymer mixture (75 μl) was then loaded into cylindrical molds (6 mm in diameter), and exposed to UV light (365 nm, 4 mW/cm^2) for 5 min to achieve gelation. Cell viability after the encapsulation was determined using a live/dead viability/cytotoxicity kit for mammalian cells (Molecular Probes). The hydrogels were incubated in osteogenic medium as previously defined [24] for 4 weeks before harvest, with medium change every 2–3 days.

RT-PCR

Total RNA was isolated from three constructs per group using Trizol method [24] and RNA from monolayer osteoblasts before encapsulation was also isolated as a control using the RNeasy Minikit. The cDNA was synthesized by RT using the Superscript First-Strand Synthesis System (Invitrogen). PCR was performed using Taq DNA Polymerase (Invitrogen) for 35 cycles and analyzed by electrophoresis on 2% agarose gels. Quantitative PCR analysis was also performed using SYBR Green detecting reagents on a Sequence Detector System (ABI 7700) and all samples were analyzed in triplicates. Relative mRNA level was calculated using the ΔΔCt methods. In brief, the expression level of every gene was first normalized to beta-actin, and results are presented as relative fold changes in the Fgfr2$^{+/S252W}$ group using normalized mRNA level in the *wild-type* group as controls. The sequences of PCR primers are listed in Table 1.

DNA content

At the end of 4 weeks of culture, three samples from each group were harvested for DNA assays as previously described [24]. Lyophilized hydrogel samples were digested using papain-PBE solution and DNA content was determined by fluorophotometry with Hoechst 33258 dye (Aldrich). Wet and dry weights after 48 h of lyophilization were obtained from all constructs for normalization of DNA content.

Histology and immunofluorescence staining

Three constructs per group were harvested for histological evaluation at the end of 4 weeks of culture. The hydrogels were fixed overnight in 4% paraformaldehyde at 4 °C and transferred to 70% ethanol until embedded in paraffin. Sections were stained with hematoxylin and eosin for examination of cell morphology. Immunofluorescence staining was performed as previously described, with rabbit polyclonal antibodies specific for collagen type I and type II (RDI) used as the primary antibodies.

In situ hybridization of the limbs from Fgfr2$^{+/S252W}$ mice

In situ hybridization was performed on neonatal day 0 mouse limb sections as described by Wilkinson (1992) [27] with modifications. The mouse osteopontin (OP) and bone sialoprotein (BSP) cDNA fragments were respectively cloned into the pCRII-TOPO® Vectors. The plasmids were linearized, sense and antisense single-stranded RNA probes were generated with T7 and SP6 RNA polymerases.

Statistical analysis

All experiments were performed in triplicate, and the results are reported as means ± standard deviation. Statistical significance was determined by analysis of variance (ANOVA single factor) and set at $p<0.05$.

Results

To confirm the osteoblast phenotype, cells isolated from the middle shaft of the long bones of Fgfr2$^{+/S252W}$ mice (Fig. 1A) and wild-type controls were stained for collagen type I during monolayer expansion. Both Fgfr2$^{+/S252W}$ and wild-type cells stained positive for collagen type I, at approximately similar levels (Figs. 1B, C).

Effects of +/S252W mutation on cell proliferation and its response to FGF ligands in monolayer culture

Osteoblasts from Fgfr2$^{+/S252W}$ mice exhibited significantly greater proliferative capacity than cells from wild-type mice during monolayer culture (Fig. 2A). The Fgfr2$^{+/S252W}$ cells showed an 81% increase in the number of proliferating cells as compared to the wild-type controls ($p<0.01$). In the presence of FGF2, cell proliferation of both Fgfr2$^{+/S252W}$ and wild-type cells increased significantly ($p<0.01$, Fig. 2A). However, the extent of the increase in cell proliferation was much greater in Fgfr2$^{+/S252W}$ cells than that in the wild-type controls. Specifically, the proliferation of the Fgfr2$^{+/S252W}$cells increased by 118% and that of the wild-type cells increased by 29% when compared to the respective controls without FGF2 ($p<0.01$). In the presence of FGF10, proliferation of the Fgfr2$^{+/S252W}$ cells increased 100%, while no significant increase was observed in the wild-type cells.

Effects of the +/S252W mutation on ALP production and its responses to FGF ligands during monolayer expansion

At day 2, Fgfr2$^{+/S252W}$ and wild-type cells produced comparable amounts of ALP (Fig. 2B). A significant increase in ALP activity per cell was observed in Fgfr2$^{+/S252W}$ cells beginning on day 4, and more ALP was produced by the mutant cells compared to the wild-type controls from day 4 to day 10. A significantly stronger ALP staining was also observed in Fgfr2$^{+/S252W}$ cells compared to wild-type cells (data not shown). For example, on days 8 and 10, the Fgfr2$^{+/S252W}$ cells respectively produced 39% and 108% more ALP, respectively, than the wild-type controls ($p<0.01$).

In the presence of 10 ng/ml FGF2, the ALP production by the Fgfr2$^{+/S252W}$ cells and wild-type cells was reduced to a negligible level (Fig. 2B). In the presence of 10 ng/ml FGF10, the ALP production by the Fgfr2$^{+/S252W}$ cells was partially inhibited (Fig. 2C). For example, compared to controls, the ALP activity of Fgfr2$^{+/S252W}$ cells decreased 59% on day 4 and 68% on day 6 ($p<0.01$). The greatest difference was observed on day 10, when Fgfr2$^{+/S252W}$ cells produced 86% less ALP in the presence of FGF10 than did control cells.

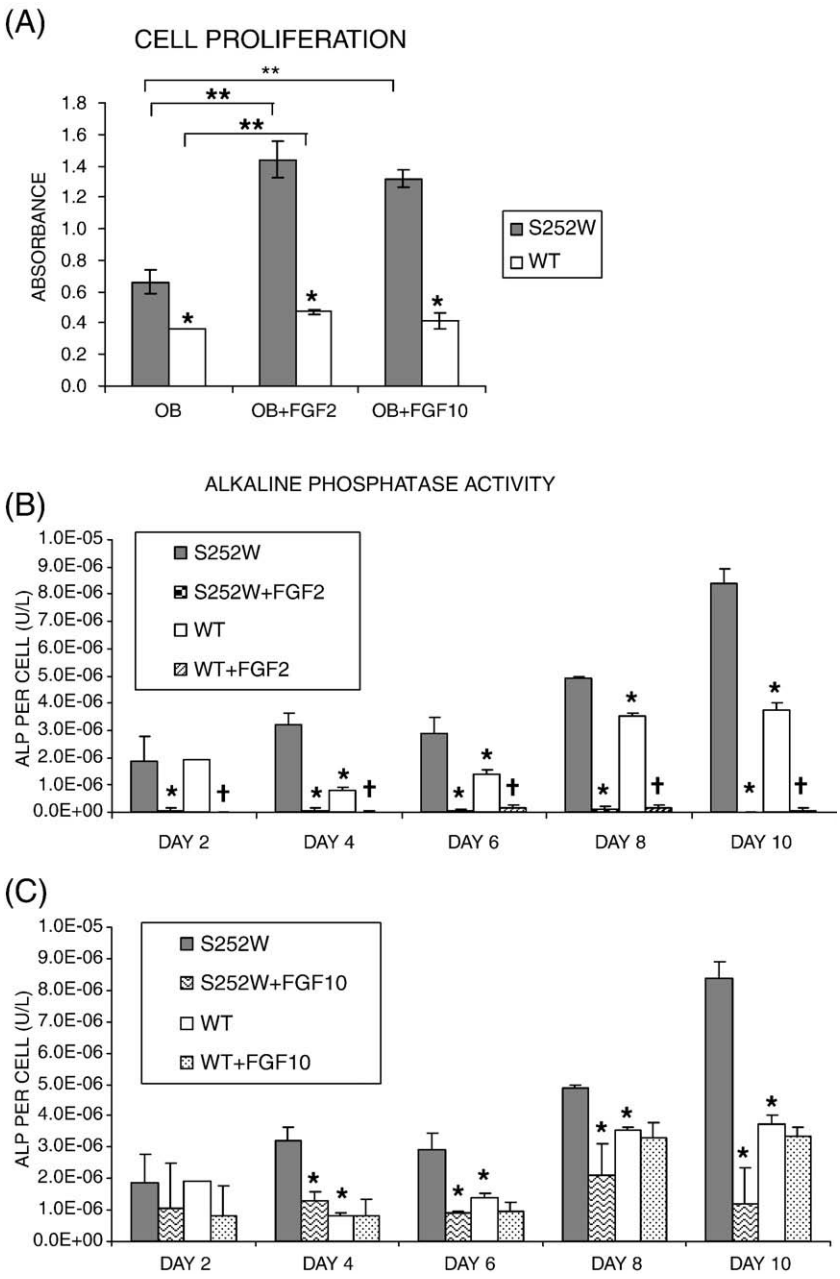

Fig. 2. Proliferation and ALP activity of isolated Fgfr2 $^{+/S252W}$ cells during monolayer expansion and their responses to FGF ligands. (A) Fgfr2$^{+/S252W}$ cells proliferated significantly faster than the wild-type controls and S252W mutation leads to altered responses in cell proliferation to FGF ligands. (B) Fgfr2$^{+/S252W}$ cells produced significantly higher amounts of ALP than the wild-type controls and FGF2 inhibited the ALP activity in both Fgfr2 $^{+/S252W}$ cells and wild-type controls. (C) FGF10 induced partial inhibition of ALP activity in Fgfr2 $^{+/S252W}$ cells, with no significant effects observed on wild-type controls. The same data set of the ALP activity of Fgfr2 $^{+/S252W}$ cells and wild-type controls in monolayer culture without growth factors was presented in (B) and (C) for additional comparison. Error bars are the standard deviations of triplicate samples (*: $p<0.01$ vs. S252W group, **: $p<0.01$ compared between two indicated groups, †: $p<0.01$ vs. WT group).

In contrast, supplementation with FGF10 did not significantly decrease the ALP activity of wild-type cells.

The +/S252W mutation leads to slight decrease in cell proliferation after 4 weeks of differentiation in 3D hydrogels

More than 95% of the osteoblasts from Fgfr2$^{+/S252W}$ mice and wild-type siblings remained viable 24 h after the encapsulation, as verified by live-dead staining (data not shown). Immediately after encapsulation, no significant difference was observed in DNA content between the Fgfr2$^{+/S252W}$ group (14.08 ± 5.95 ng/mg) and the wild-type control (17.30 ± 1.95 ng/mg) (Fig. 3A). DNA content within the hydrogels increased slightly over the 4 weeks of culture. At the end of 4 weeks in culture, the DNA content in the Fgfr2$^{+/S252W}$ group (18.17 ± 0.44) was 14% lower than that of the wild-type control (21.23 ± 0.69), with $p<0.01$. After 4 weeks of culture in osteogenic medium, the water content of the Fgfr2$^{+/S252W}$ gels (83.3 ± 0.3%) was the same as that of the wild-type gels (83.2 ± 0.8%), indicating the same pore size and physical property of the hydrogels for both groups.

The +/S252W mutation leads to increased collagen type I deposition and abnormal chondrogenesis after 3D differentiation

Immunofluorescence staining for collagen type I was positive in both Fgfr2$^{+/S252W}$ gels and wild-type controls by the end of 4-weeks culture under osteogenic conditions (Figs. 3B, C). A stronger staining of

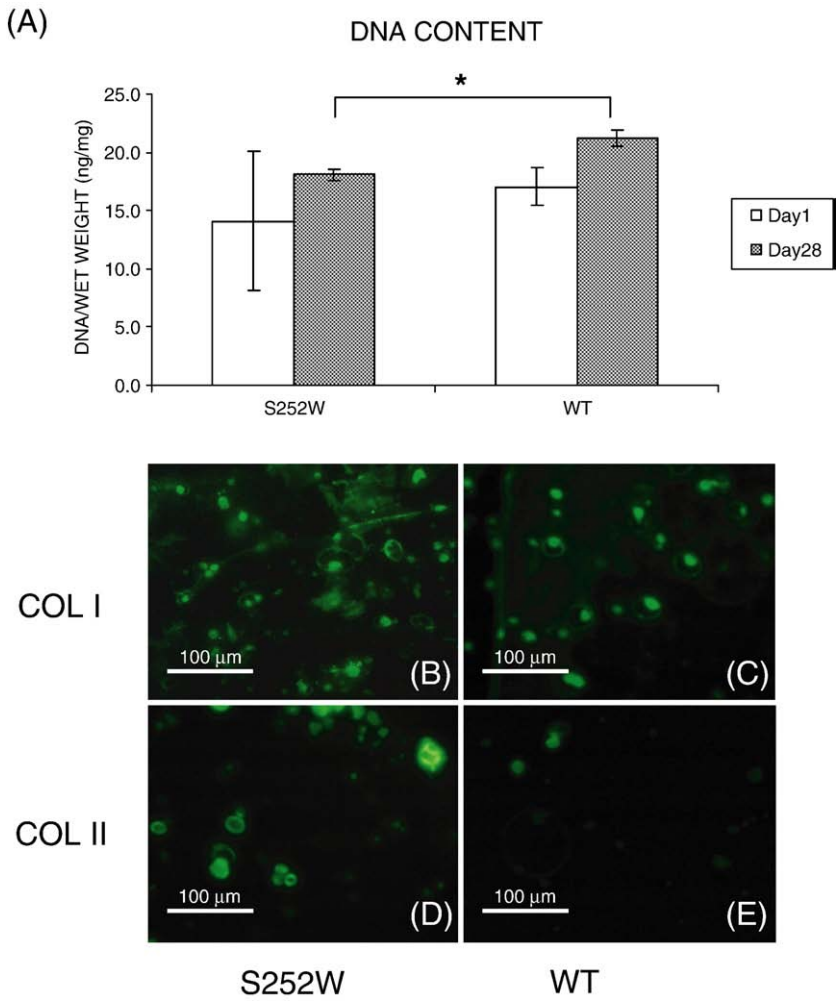

Fig. 3. Proliferation and collagen deposition of Fgfr2 $^{+/S252W}$ cells in hydrogel culture. (B, D) mutant cells; (C, E) wild-type controls. (A) Proliferation is reflected by DNA content at day 1 after encapsulation and day 28 at harvest. Error bars are the standard deviations of triplicate samples (*: $p<0.01$ vs. WT). (B, C) After 28 days of culture under osteogenic conditions, immunofluorescence staining of collagen type I showed increased deposition by mutant cells in hydrogels. (D, E) Strong staining of cartilage specific marker, collagen type II, was observed in the mutant group while only minimal staining was seen in the wild-type controls. Scale bars: B–E, 100 μm.

collagen type I was observed in the Fgfr2$^{+/S252W}$ gels compared to the wild-type controls. Strong staining of cartilage specific marker, collagen type II, was observed in the cellular and pericellular regions in the Fgfr2$^{+/S252W}$ group while only minimal staining was seen in the wild-type controls, as we have previously reported *in vivo* (Figs. 3D, E) [11].

The +/S252W mutation leads to upregulation of bone marker genes and down-regulation of bone remodeling gene expression after 3D osteogenic differentiation

After 4 weeks of culture in osteogenic medium, Fgfr2$^{+/S252W}$ cells expressed significantly higher levels of most bone markers than wild-type control cells, as demonstrated by quantitative PCR (Figs. 4A–F). For example, the expression levels of Cbfa-1 and bone sialoprotein were respectively 93% and 52% higher in the Fgfr2$^{+/S252W}$ cells than the wild-type control cells ($p<0.01$). The same trend was observed with regards to osteopontin and osteonectin, although the differences were not statistically significant. Fgfr2$^{+/S252W}$ cells expressed 2.8-fold more collagen type 1 and 3.3-fold more osteocalcin than did wild-type control cells. Meanwhile, Fgfr2$^{+/S252W}$ cells demonstrated significantly decreased expressions of bone remodeling genes. Specifically, Fgfr2$^{+/S252W}$ cells expressed 87% less MMP-13, 71% less Noggin, and 75% less BMP4 than did the wild-type control cells, as shown by quantitative PCR (Figs. 4G–I).

The +/S252W mutation leads to increased osteopontin expression and mineralization in mouse limbs in vivo

Detection of mouse osteopontin by *in situ* hybridization on neonatal (day 0) mouse limb sections revealed higher expression of this early bone marker in the limbs of the Fgfr2$^{+/S252W}$ mice compared to the wild-type control mice (Figs. 5A, B). At this stage, no significant difference was observed in the expression levels of bone sialoprotein (BSP), a late bone marker (Figs. 5C, D). Alizarin red S staining on day 0 mouse limb sections also exhibited higher amounts of mineralization in the long bone regions of Fgfr2$^{+/S252W}$ mice compared to the wild-type controls (Figs. 5E, F).

Discussion

In the present study, we utilized a tissue culture model initially developed for tissue engineering to analyze the quantitative effects of Fgfr2$^{+/S252W}$ mutation on bone development. After 4 weeks of culture in osteogenic medium, Fgfr2$^{+/S252W}$ cells in 3D gels showed an increased osteoblastic differentiation phenotype compared to the wild-type controls, as indicated by a significant upregulation of the expression of late bone markers including collagen type I, bone sialoprotein and osteocalcin. Consistent with our 3D findings in hydrogel culture, limb sections of the day 0 neonatal Fgfr2$^{+/S252W}$ mice demonstrated increased expression of early bone marker osteopontin and higher

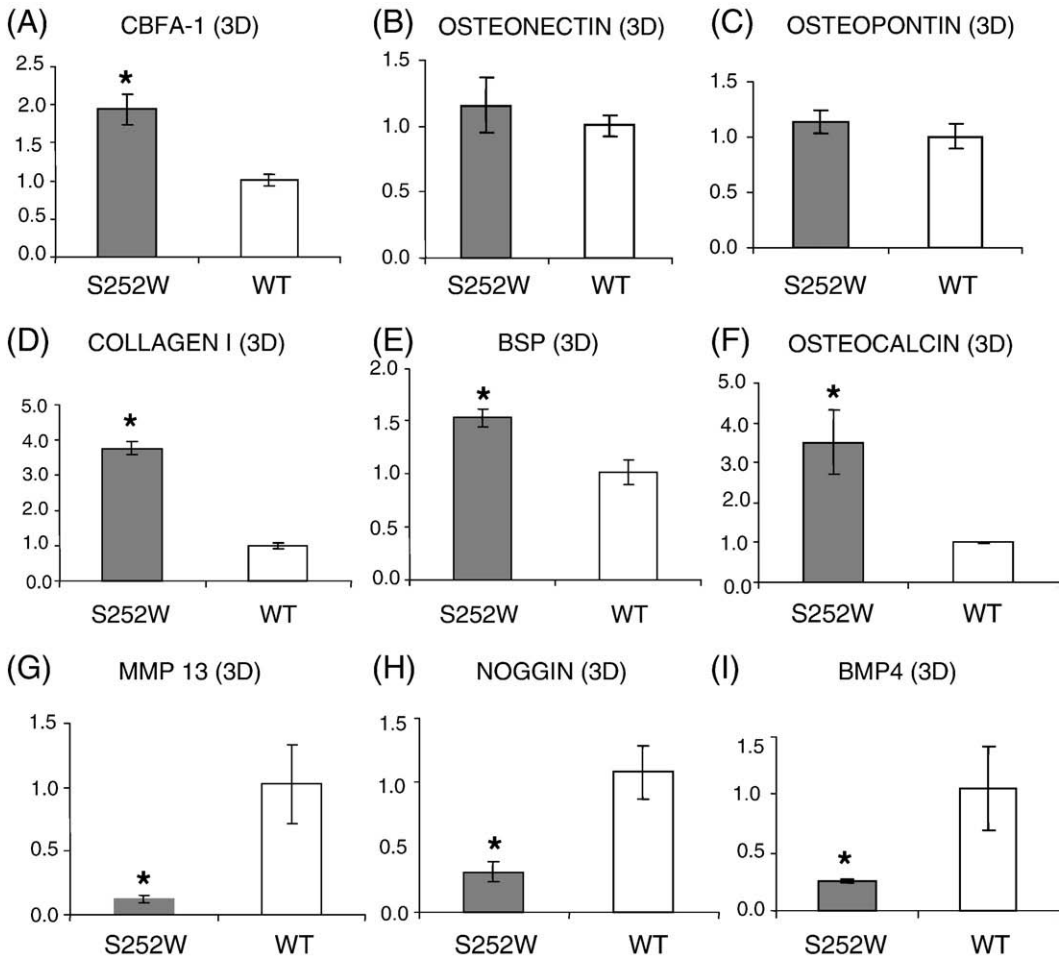

Fig. 4. Normalized gene expressions of osteogenesis and bone remodeling markers by quantitative PCR of Fgfr2 $^{+/S252W}$ cells and wild-type controls in 3D hydrogel after 4 weeks of culture in osteogenic medium. Results are presented as relative fold changes in the Fgfr2$^{+/S252W}$ group using ΔΔCt method, with normalized mRNA level in the wild-type group as a control. Error bars are the standard deviations of triplicate samples (*: $p<0.01$ vs. WT).

degree of mineralization than in the wild-type controls. Furthermore, our data suggest several mechanisms that may underlie the abnormal bone development associated with Apert syndrome, such as increased osteoblastic differentiation, decreased bone matrix remodeling, and altered cellular responses to FGF ligands with different specificity.

The cells used in this study were extracted from bone and are primarily composed of osteoblasts. We chose the current scaffolds as numerous studies have used 3D hydrogel scaffolds to culture osteoblasts or osteogenic cells for bone repair purposes, with documentation of these 3D scaffolds promoting osteoblastic differentiation and bone matrix formation [28–31]. One advantage of the 3D photopolymerizable hydrogel system is its capacity to homogeneously encapsulate cells. We have previously shown that the cell distribution and tissue growth is uniform throughout the 3D hydrogel by histology [11]. When osteoblasts from Fgfr2$^{+/S252W}$ mice were cultured in hydrogels, which simulates a 3D physiological environment, the cells underwent active osteogenesis. After 4 weeks of culture in 3D in osteogenic medium, a significant upregulation of all three bone markers including collagen type I, bone sialoprotein and osteocalcin was found in Fgfr2$^{+/S252W}$ osteoblasts. A previous clinical study by De Pollack et al. also reported increased ALP activity and osteocalcin production by osteoblastic cells isolated from fused sutures compared with cells isolated from normal sutures in the same patients [14]. Both their results and our results suggest that Fgfr2$^{+/S252W}$ mutation is associated with increased osteoblastic differentiation in both intramembranous and endochondral bone formation. For tissue engineering applications, the scaffold properties can often influence cell behavior such as the amount of matrix production. Although the absolute amount of matrix may depend on scaffolds, the differences of the matrix production between the mutant and the wild-type cells would still be similar. Cell–cell communication is also a critical issue and can be achieved through direct cell–cell contact or diffusion of soluble factors. In our model system, the encapsulated cells are not in direct contact while the hydrogel allows the soluble factors to diffuse across the gel and is adaptable to form multi-layer hydrogels [32].

In contrast to the significantly increased BSP expression we observed in the Fgfr2$^{+/S252W}$ cells after 4 weeks of *in vitro* culture under osteogenic conditions, the *in situ* hybridization results did not show significant differences in the BSP expression between the Fgfr2$^{+/S252W}$ mouse limb sections and the controls. This could be explained by the different cell maturation stages at which the gene expression patterns were examined. *In situ* hybridization was performed with the P0 mouse limb sections, which represented the initial stage at which the cells were isolated. In contrast, the quantitative PCR analyses were completed after the cells were cultured in 3D under osteogenic conditions for 4 weeks and had reached a more mature cell stage. Our 3D PCR analyses demonstrated a greater increase in the expressions of mature bone markers (bone sialoprotein, osteocalcin, collagen type I) while the *in situ* hybridization results showed a greater increase in the expression of early bone marker (osteopontin). These findings suggest this *in vitro* 3D model is an effective tool to study the cell and tissue development at a more mature stage, and is particularly useful for evaluating disease development where the animal model is neonatal lethal.

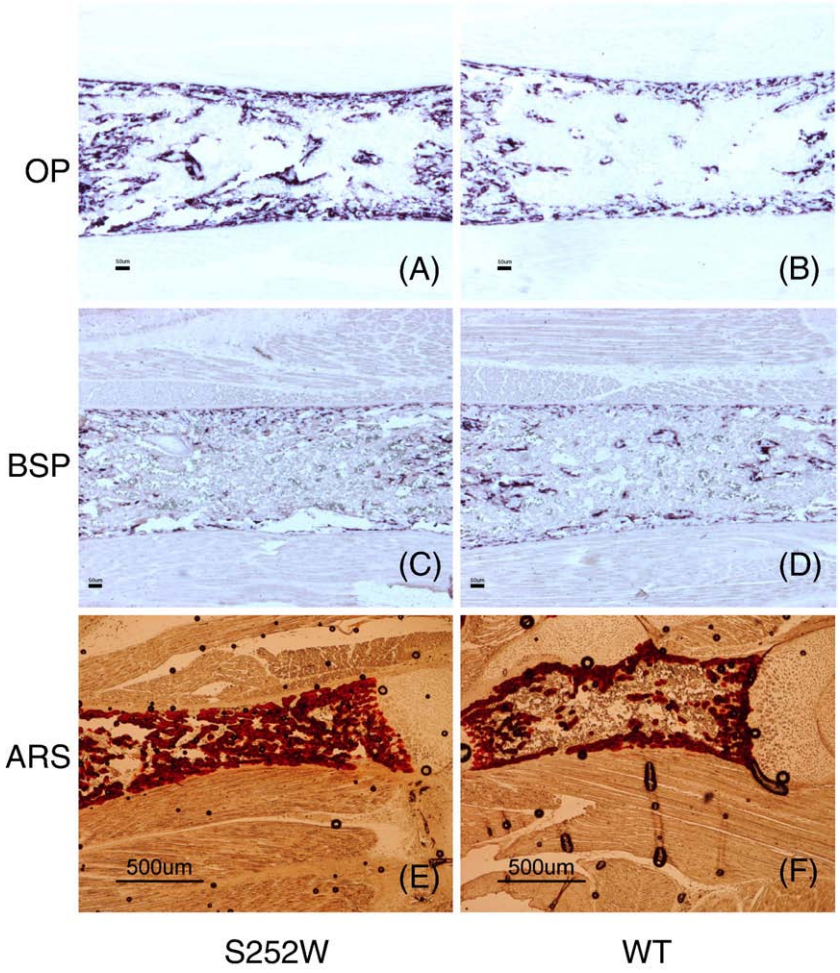

Fig. 5. *In situ* hybridization and alizarin red S (ARS) staining in P0 Fgfr2$^{+/S252W}$ middle shaft of the mouse limb sections. (A, C, E) mutant mice; (B, D, F) control littermates. (A, B) *In situ* hybridization of osteopontin (OP) showed increased expression in the mutant mice. (C, D) No significant differences were observed in bone sialoprotein (BSP) expression between the mutant and control at P0. (E, F) Increased ARS staining showed more mineralization in the mutant group. Scale bars: A–D, 50 μm; E,F, 500 μm.

Fgfr2$^{+/S252W}$ cells proliferated significantly faster than wild-type control cells in monolayer culture. This finding is consistent with a previous monolayer study by Mansukhani et al., in which FGFR2 S252W transfected osteoblasts exhibited a two-fold increase in proliferation [13]. The hydrogel we used did not encourage cell proliferation and the cell number only increased slightly over 4-weeks culture period. This better mimics the *in vivo* scenario, where the differentiating osteoblasts do not actively proliferate. Furthermore, the slightly decreased cell proliferation in hydrogel culture is accompanied by an increased osteoblastic cell differentiation in Fgfr2$^{+/S252W}$ cells at the end of the 4-week culture. This is in line with previous reports in which more mature osteoblasts demonstrated a lower proliferative capacity [13,33].

To investigate the cellular mechanism that links the S252W mutation to the observed alterations in osteoblastic differentiation, we evaluated the changes in the FGFR2 responses to FGF ligands by examining cell proliferation and ALP production. We specifically chose FGF2 and FGF10, two ligands that are reported to have different binding specificity to FGFR2 [8]. Osteoblasts we used in this study express the Fgfr2c splice form. FGF2 normally binds to Fgfr2c, and our results indicated that both mutant and wild-type cells responded to FGF2 with increased cell proliferation and decreased ALP production. However, the increase in cell proliferation of the mutant cells (118%) was much greater than that of the wild-type cells (29%) when both were exposed to the same concentration of FGF2 ($p<0.01$). The mechanisms by which the S252W mutation increased responses of cell proliferation to FGF2 remain unclear. One possibility is the increased affinity of FGF2 to the S252W mutant Fgfr2c, as S252W mutation decreases the ligand/receptor dissociation rate and prolonged binding [7]. Alternatively, S252W mutation may produce an increased response in the intracellular pathways that affect the cell proliferation.

The S252W mutation has also been shown to alter FGFR2 binding specificity for various FGF ligands [8,9,34]. Crystal structure analyses of Fgfr2c demonstrated that S252W mutation may allow Fgfr2c to abnormally bind FGF ligands, such as FGF7 and FGF10 [8,34]. In another study, S252W mutation in Fgfr2c showed robust tyrosine phosphorylation in response to FGF7 while wild-type Fgfr2c was not phosphorylated after addition of FGF7 [9]. We indeed observed the response of Fgfr2$^{+/S252W}$ osteoblasts to FGF10, with an increase in cell proliferation and partial inhibition in alkaline phosphatase production. Our results indicate that the S252W mutation not only allows FGF10 to bind and activate Fgfr2c, but it also affects the signal transduction pathways that are involved in alkaline phosphatase production.

Metalloprotease-13 (MMP-13) is a protease that plays an essential role in extracellular matrix remodeling [35]. Our results showed a downregulation of MMP-13 in Fgfr2$^{+/S252W}$ osteoblasts, in both monolayer and hydrogel culture. MMP-13 downregulation was previously reported in a study of FGFR2 with the P253R mutation, another substitution in Fgfr2 that is associated with Apert syndrome [35]. Such alterations may disturb the delicate balance among various extracellular matrix components and cause abnormalities in skeletal development. In fact, this speculation is supported by our 3D culture results, in which downregulation of MMP-13 was accompanied by

significant upregulation of bone matrix proteins collagen type I, bone sialoprotein and osteocalcin. The same trend was observed in the expression of Noggin, an antagonist of BMPs, for which a significant downregulation was observed in hydrogel culture. Downregulation of Noggin has been proposed as one of the mechanism of Fgfr-mediated craniosynostosis [36]. The BMP4 expression pattern was the same as Noggin. However, further detailed investigations are required to determine the regulation of other members of the BMP family in the context of this mutation.

In the present study, we saw a notable level of expression of the cartilage marker collagen type II in the $FGFR2^{+/S252W}$ cells in hydrogel culture under osteogenic conditions, whereas only minimum staining was seen in the controls. Abnormal chondrogenesis was previously observed in the craniofacial and other organs of our mutant mice [11]. Clinically, ectopic chondrogenesis has been observed in periarticular tissues of Apert syndrome digits [37]. Thus, the S252W mutation may be involved in the regulation of cell fate determinants and/or proliferation that affect chondrogenesis in addition to osteogenesis.

Mouse calvarial organ culture system has been used previously to study Apert syndrome. It was shown that FGF2-induced osteogenic response can be blocked by the addition of FGFR2IIIcS252W [38]. While organ explant culture provides a very useful tool to study the disease phenotype, our 3D culture offer additional advantages that cannot be achieved by organ culture. Most notably, the 3D *in vitro* culture model enable us to have better control of experimental parameters, such as cell density, cell types, and the matrix components, which will greatly enhance our capability to dissect the disease mechanisms. Specifically, when certain responses are observed through the organ culture, it can be difficult to identify which factor is responsible for the observation as organ culture integrates all the factors (cell–cell interactions, matrix factors, secreted soluble factors etc.). In contrast, the 3D culture model would allow us to examine the effects of multiple factors individually or in any possible combinations. For example, the 3D hydrogel model would enable the examination of cell–cell interactions by co-culturing different cell types in multilayered hydrogels in a defined manner. Furthermore, *in vitro* culture system would allow expansion of the cells from the explant materials, which would potentially allow more assays to be performed.

In summary, this study has applied tissue engineering strategies to study the genetic disease, Apert syndrome, which leads to abnormal bone development. In the 3D hydrogel culture model, the $FGFR2^{+/S252W}$ mutation was associated with increased osteoblastic differentiation, decreased bone matrix remodeling and abnormal chondrogenesis. The correlation between *in vitro* data and *in vivo* findings has provided the basis for proposing this *in vitro* 3D culture system as a valuable alternative method for future studies of the determinants of both normal and abnormal skeletal development. It has the potential to lead to a significant improvement in our understanding of the pathophysiological process associated with Apert syndrome and other genetic diseases, which often are lethal mutations in animal models. Furthermore, although knock-out and conditional targeting technologies are available, they are not practical to human and our 3D culture model would be particularly valuable in handling human materials.

Conflict of interest

All authors have no conflicts of interest.

Acknowledgments

This work was supported by NIH/NIDCR DE016887 (J.H.E.).

References

[1] Chen L, Deng CX. Roles of FGF signaling in skeletal development and human genetic diseases. Front Biosci 2005;10:1961–76.
[2] Ornitz DM, Marie PJ. FGF signaling pathways in endochondral and intramembranous bone development and human genetic disease. Genes Dev 2002;16:1446–65.
[3] Cohen Jr MM, Kreiborg S, Lammer EJ, Cordero JF, Mastroiacovo P, Erickson JD, Roeper P, Martinez-Frias ML. Birth prevalence study of the Apert syndrome. Am J Med Genet 1992;42:655–9.
[4] Cohen Jr MM, Kreiborg S. New indirect method for estimating the birth prevalence of the Apert syndrome. Int J Oral Maxillofac Surg 1992;21:107–9.
[5] Wilkie AO, Slaney SF, Oldridge M, Poole MD, Ashworth GJ, Hockley AD, Hayward RD, David DJ, Pulleyn LJ, Rutland P. Apert syndrome results from localized mutations of FGFR2 and is allelic with Crouzon syndrome. Nat Genet 1995;9:165–72.
[6] Park WJ, Theda C, Maestri NE, Meyers GA, Fryburg JS, Dufresne C, Cohen Jr MM, Jabs EW. Analysis of phenotypic features and FGFR2 mutations in Apert syndrome. Am J Hum Genet 1995;57:321–8.
[7] Anderson J, Burns HD, Enriquez-Harris P, Wilkie AO, Heath JK. Apert syndrome mutations in fibroblast growth factor receptor 2 exhibit increased affinity for FGF ligand. Hum Mol Genet 1998;7:1475–83.
[8] Yu K, Herr AB, Waksman G, Ornitz DM. Loss of fibroblast growth factor receptor 2 ligand-binding specificity in Apert syndrome. Proc Natl Acad Sci U S A 2000;97:14536–41.
[9] Ibrahimi OA, Zhang F, Eliseenkova AV, Itoh N, Linhardt RJ, Mohammadi M. Biochemical analysis of pathogenic ligand-dependent FGFR2 mutations suggests distinct pathophysiological mechanisms for craniofacial and limb abnormalities. Hum Mol Genet 2004;13:2313–24.
[10] Arman E, Haffner-Krausz R, Chen Y, Heath JK, Lonai P. Targeted disruption of fibroblast growth factor (FGF) receptor 2 suggests a role for FGF signaling in pregastrulation mammalian development. Proc Natl Acad Sci U S A 1998;95:5082–7.
[11] Wang Y, Xiao R, Yang F, Karim BO, Iacovelli AJ, Cai J, Lerner CP, Richtsmeier JT, Leszl JM, Hill CA, Yu K, Ornitz DM, Elisseeff J, Huso DL, Jabs EW. Abnormalities in cartilage and bone development in the apert syndrome FGFR2(+/S252W) mouse. Development 2005;132:3537–48.
[12] Chen L, Li D, Li C, Engel A, Deng CX. A Ser252Trp substitution in mouse fibroblast growth factor receptor 2 (Fgfr2) results in craniosynostosis. Bone 2003;33:169–78.
[13] Mansukhani A, Bellosta P, Sahni M, Basilico C. Signaling by fibroblast growth factors (FGF) and fibroblast growth factor receptor 2 (FGFR2)-activating mutations blocks mineralization and induces apoptosis in osteoblasts. J Cell Biol 2000;149:1297–308.
[14] De Pollack C, Renier D, Hott M, Marie PJ. Increased bone formation and osteoblastic cell phenotype in premature cranial suture ossification (craniosynostosis). J Bone Miner Res 1996;11:401–7.
[15] Chun TH, Hotary KB, Sabeh F, Saltiel AR, Allen ED, Weiss SJ. A pericellular collagenase directs the 3-dimensional development of white adipose tissue. Cell 2006;125:577–91.
[16] Cukierman E, Pankov R, Stevens DR, Yamada KM. Taking cell–matrix adhesions to the third dimension. Science 2001;294:1708–12.
[17] Bissell MJ, Radisky D. Putting tumours in context. Nat Rev Cancer 2001;1:46–54.
[18] Walpita D, Hay E. Studying actin-dependent processes in tissue culture. Nat Rev Mol Cell Biol 2002;3:137–41.
[19] Grinnell F. Fibroblast biology in three-dimensional collagen matrices. Trends Cell Biol 2003;13:264–9.
[20] Yamada KM. Cell biology: tumour jailbreak. Nature 2003;424:889–90.
[21] Boudreau N, Weaver V. Forcing the third dimension. Cell 2006;125:429–31.
[22] Hotary KB, Allen ED, Brooks PC, Datta NS, Long MW, Weiss SJ. Membrane type I matrix metalloproteinase usurps tumor growth control imposed by the three-dimensional extracellular matrix. Cell 2003;114:33–45.
[23] Elisseeff J, Anseth K, Sims D, McIntosh W, Randolph M, Langer R. Transdermal photopolymerization for minimally invasive implantation. Proc Natl Acad Sci U S A 1999;96:3104–7.
[24] Yang F, Williams CG, Wang DA, Lee H, Manson PN, Elisseeff J. The effect of incorporating RGD adhesive peptide in polyethylene glycol diacrylate hydrogel on osteogenesis of bone marrow stromal cells. Biomaterials 2005;26:5991–8.
[25] Williams CG, Kim TK, Taboas A, Malik A, Manson P, Elisseeff J. In vitro chondrogenesis of bone marrow-derived mesenchymal stem cells in a photopolymerizing hydrogel. Tissue Eng 2003;9:679–88.
[26] McLeod MJ. Differential staining of cartilage and bone in whole mouse fetuses by alcian blue and alizarin red S. Teratology 1980;22:299–301.
[27] Wilkinson DG. In situ hybridization: a practical approach. London, UK: Oxford University Press; 1992.
[28] Shin H, Zygourakis K, Farach-Carson MC, Yaszemski MJ, Mikos AG. Modulation of differentiation and mineralization of marrow stromal cells cultured on biomimetic hydrogels modified with Arg-Gly-Asp containing peptides. J Biomed Mater Res A 2004;69:535–43.
[29] Trojani C, Weiss P, Michiels JF, Vinatier C, Guicheux J, Daculsi G, Gaudray P, Carle GF, Rochet N. Three-dimensional culture and differentiation of human osteogenic cells in an injectable hydroxypropylmethylcellulose hydrogel. Biomaterials 2005;26:5509–17.
[30] Benoit DS, Durney AR, Anseth KS. Manipulation in hydrogel degradation behavior enhance osteoblasts function and mineralized tissue formation. Tissue Eng 2006;12:1663–73.
[31] Chung EH, Gilbert M, Virdi AS, Sena K, Sumner DR, Healy KE. Biomimetic artificial ECMs stimulate bone regeneration. J Biomed Mater Res A 2006;79:815–26.
[32] Sharma B, Elisseeff JH. Engineering structurally organized cartilage and bone tissues. Ann Biomed Eng 2004;32(1):148–59.
[33] Owen TA, Aronow M, Shalhoub V, Barone LM, Wilming L, Tassinari MS, Kennedy MB, Pockwinse S, Lian JB, Stein GS. Progressive development of the rat osteoblast phenotype in vitro: reciprocal relationships in expression of genes associated with

osteoblast proliferation and differentiation during formation of the bone extracellular matrix. J Cell Physiol 1990;143:420–30.
[34] Plotnikov AN, Hubbard SR, Schlessinger J, Mohammadi M. Crystal structures of two FGF–FGFR complexes reveal the determinants of ligand-receptor specificity. Cell 2000;101:413–24.
[35] Baroni T, Carinci P, Lilli C, Bellucci C, Aisa MC, Scapoli L, Volinia S, Carinci F, Pezzetti F, Calvitti M, Farina A, Conte C, Bodo M. P253R fibroblast growth factor receptor-2 mutation induces RUNX2 transcript variants and calvarial osteoblast differentiation. J Cell Physiol 2005;202:524–35.
[36] Warren SM, Brunet LJ, Harland RM, Economides AN, Longaker MT. The BMP antagonist noggin regulates cranial suture fusion. Nature 2003;422:625–9.
[37] Holten IW, Smith AW, Bourne AJ, David DJ. The Apert syndrome hand: pathologic anatomy and clinical manifestations. Plast Reconstr Surg 1997;99:1681–7.
[38] Tanimoto Y, Yokozeki M, Hiura K, Matsumoto K, Nakanishi H, Matsumoto T, Marie PJ, Moriyama K. A soluble form of fibroblast growth factor receptor 2 (FGFR2) with S252W mutation acts as an efficient inhibitor for the enhanced osteoblastic differentiation caused by FGFR2 activation in Apert syndrome. J Biol Chem 2004;279(44):45926–34.